

ENERGY LOSS MECHANISMS OF ROCKING BLOCKS: EXPERIMENTAL OBSERVATIONS

Georgios Vlachakis¹, Carla Colombo¹, Anastasios I. Giouvanidis², Nuno Mendes¹,
Nathanaël Savalle³, Paulo B. Lourenço¹

¹ University of Minho, ISE, ARISE, Department of Civil Engineering, 4800-058 Guimarães,
Portugal
E-mail: carla.colombo95@gmail.com, giorgovlachaki@gmail.com, nunomendes@civil.uminho.pt,
pbl@civil.uminho.pt

² Department of Civil Engineering, University of Nottingham, University Park, NG7 2RD
Nottingham, United Kingdom
E-mail: anastasios.giouvanidis@nottingham.ac.uk

³ Université Clermont Auvergne, Clermont Auvergne INP, CNRS, Institut Pascal
F-63000 Clermont-Ferrand, France
E-mail: nathanael.savalle@uca.fr

Abstract

A variety of different structures experience rocking motion when subjected to dynamic actions, making rocking dynamics a fundamental problem of earthquake engineering. Rocking motion presents peculiar dynamic characteristics, such as negative stiffness during pivoting and non-smooth phenomena during impacts. Hence, modelling of the rocking problem faces significant challenges. One of the most significant is related to the energy losses that occur during impacts, commonly represented by the coefficient of restitution. Despite the numerous theoretical attempts to accurately estimate the coefficient of restitution, it is apparent that experimental observations are essential in providing a direct insight into the complex and non-smooth phenomena of rocking motion. To this end, the present work conducts an extended experimental campaign on the free-rocking motion of limestone blocks. More specifically, a total of 36 blocks are tested, corresponding to 12 different geometrical aspect ratios. The free-rocking motion is thoroughly analysed, while attention is also given to three-dimensional effects. Finally, the coefficient of restitution is experimentally quantified and compared with both previous theoretical and experimental results gathered from the literature.

Keywords: Rocking Motion, Coefficient of Restitution, Experimental Campaign, Free-rocking, Masonry, Digital Image Correlation

1 INTRODUCTION

The dynamic behaviour of a block rocking freely on its base constitutes a fundamental, yet challenging, problem of nonlinear dynamics and earthquake engineering, as it reflects the basic dynamic response of a variety of structures, such as buildings [1,2], bridges [3–8], classical monuments [9,10], non-structural elements [11], statues [12,13] etc. In particular, with respect to masonry structures, rocking behaviour becomes evident when the façades experience out-of-plane deformations due to lack of sufficient (or preliminarily fractured) connections with the adjacent walls [14,15]. In fact, such a collapse mechanism has been observed to be the most decisive and recurrent type of failure for masonry buildings after actual seismic events [16,17].

In general, the dynamics of a rocking block differs from the classical single-degree-of-freedom oscillator and present peculiar characteristics [18,19]. In essence, the rocking motion is composed of two phases: i) the pivoting over each corner, and ii) the impacts with the base when alternating the corners of pivoting. Firstly, the pivoting phase is smooth (although nonlinear due to the negative stiffness of the system), while impacts are non-smooth, impulsive and lead to energy losses. As a result, the pivoting phase is usually adequately described when using geometrically nonlinear models [20], while impacts are burdensome to model explicitly [21–23]. Therefore, impacts are commonly treated in a phenomenological sense by studying the time instants immediately before and after each impact, while considering the energy losses with the Coefficient of Restitution (CoR) [24].

Clearly, the CoR has a crucial role when modelling the rocking motion numerically, though its estimation is non-trivial. It may be estimated by using either theoretical assumptions or experimental observations [25]. In more detail, the first theoretical approach to compute the CoR was proposed by Housner [24], who assumed pure rocking motion (i.e. no sliding or bouncing), and computed the CoR using the conservation of angular momentum. Later, the research provided significant contributions in this theoretical framework by alleviating most assumptions [26–29]. Nevertheless, the general formulation of the problem appears to introduce undefined parameters that need to be experimentally or geometrically specified. On the contrary, experimental investigations of the CoR allow its direct quantification [30]. In this case, assumptions are omitted while the physical complexities of the problem are revealed. Indicatively, experimental investigations have shown the importance of bouncing [31], sliding [32], three-dimensional motion [33], the role of interface and material properties [34–37], and/or the influence of geometrical imperfections and irregularities [38]. Nevertheless, experimental studies are notably sparse, usually limited to few geometrical aspect ratios, while three-dimensional recording is often lacking.

The objective of this study is to provide an experimental insight into the energy losses of rocking motion and investigate the impact of three-dimensional effects on the global rocking response. To this end, a total of 36 free-rocking tests are conducted and analysed using 36 different limestone blocks of 12 different geometrical aspect ratios, i.e. height over width ratios. Attention is also given to the three-dimensional response of the rocking blocks, which is measured with a state-of-the-art contactless technique. Furthermore, the dependence of the CoR on the rocking amplitude and aspect ratio is presented and discussed.

The paper is structured as follows: the present section (Section 1) introduces the research significance and objectives of the work. Section 2 presents the theoretical framework of rocking dynamics, while Section 3 describes the experimental campaign. Section 4 first provides a detailed discussion of the outcomes of a representative free-rocking test, which is followed by the illustration of the CoR results for all the 36 tests. Finally, Section 5 concludes the work by highlighting the main observations.

2 THEORETICAL ROCKING DYNAMICS

Consider a block with height H and width B that experiences planar rocking motion on its base (Figure 1a). The rocking motion may be described using rigid body dynamics. Thus, the equation of motion writes [24]:

$$\ddot{\theta}_{xx} = -p^2 \left[\sin(\pm\alpha - \theta_{xx}) + \frac{\ddot{u}_g}{g} \cos(\pm\alpha - \theta_{xx}) \right] \quad (1)$$

where θ_{xx} describes the rocking rotation, α is the critical slenderness angle of the block (i.e. $\alpha = \tan^{-1}(H/B)$), p is the frequency parameter of the block, defined as $p = \sqrt{mgR/I_0}$, with m representing the mass, I_0 the rotational moment of inertia with respect to the pivot points and R the diagonal distance of the centre of mass to the pivot points, g is the acceleration of gravity and \ddot{u}_g is the base (ground) acceleration. Finally, the signum \pm refers to the sign of the rocking angle θ_{xx} with the upper sign corresponding to clockwise and the bottom to counter-clockwise rotations. Note that Eq. (1) is non-linear and thus the period T of rocking motion is amplitude dependent [24]:

$$T = \frac{4}{p} \cosh^{-1} \left[1 / \left(1 - \frac{\theta_{xx,0}}{\alpha} \right) \right] \quad (2)$$

where $\theta_{xx,0}$ is the amplitude of the rocking angle θ_{xx} .

Furthermore, assuming pure rocking behaviour (i.e. no sliding and bouncing), the two energy components of rocking motion, i.e. the Potential $E_{\text{POTENTIAL}}$ and Kinetic E_{KINETIC} energies, compose the Total energy E_{TOTAL} that read respectively:

$$E_{\text{POTENTIAL}} = mgR \left[\cos(\alpha - |\theta_{xx}|) - \cos \alpha \right] \quad (3)$$

$$E_{\text{KINETIC}} = \frac{1}{2} I_0 \dot{\theta}_{xx}^2 \quad (4)$$

$$E_{\text{TOTAL}} = E_{\text{POTENTIAL}} + E_{\text{KINETIC}} \quad (5)$$

Equation (1) represents the smooth part of rocking motion, i.e. when pivoting, while non-smooth impacts occur when the block changes pivot point, i.e. when $\theta_{xx} = 0$. Those impacts occur over finite, but extremely short, time periods and result in energy losses. An accurate description of the impacts is commonly omitted, in favour of a phenomenological treatment using the CoR [39]. More specifically, the post-impact angular velocity $\dot{\theta}^+$ is related to the pre-impact $\dot{\theta}^-$ using the CoR: $e = \dot{\theta}^+ / \dot{\theta}^-$. Assuming no bouncing or sliding, Housner [24] estimated the CoR using the conservation of angular momentum before and after impact, yielding:

$$e = 1 - \frac{3}{2} \sin^2 \alpha \quad (6)$$

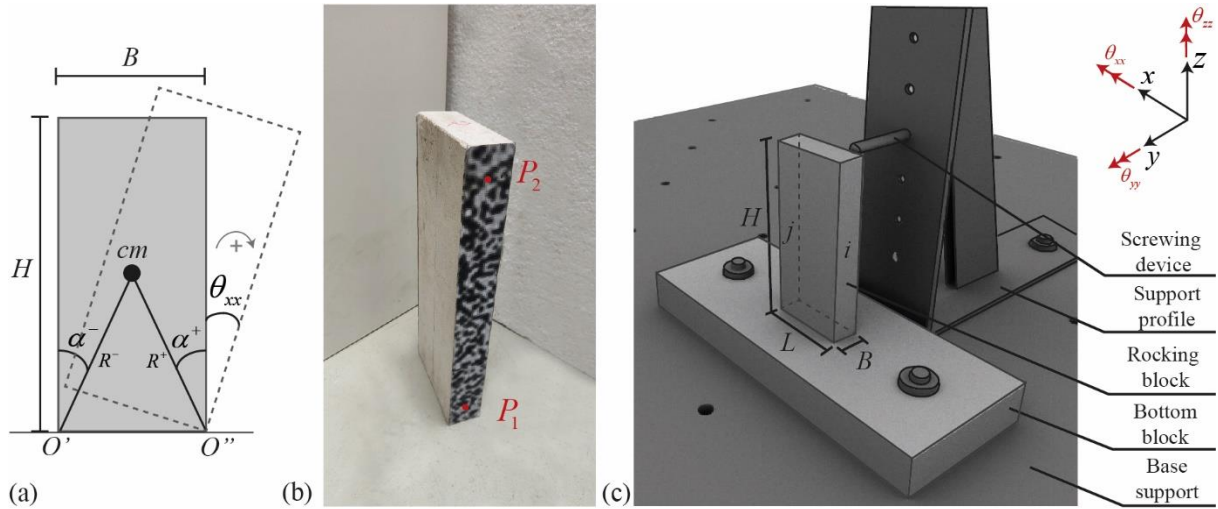


Figure 1: (a) Schematic view of the planar asymmetric rocking block, (b) limestone block with the speckle pattern used by the Digital Image Correlation (DIC) system, and (c) schematic 3D drawing of the free-rocking experimental setup.

Note that according to Housner's theory [24], the CoR (Eq. (6)) depends solely upon the geometry of the block, and thus the material properties are assumed irrelevant to the overall damping of the system.

3 FREE-ROCKING EXPERIMENTAL CAMPAIGN

The free-rocking tests are performed on limestone parallelepiped blocks (Figure 1b) of density $\rho = 2238 \text{ kg/m}^3$ and elastic modulus $E = 32.7 \text{ GPa}$ [40]. All the blocks have common nominal dimensions in plan ($B = 50 \text{ mm}$ and $L = 150 \text{ mm}$, $L/B = 3$), while their height H spans from 200 mm to 750 mm with steps of 50 mm, resulting in 12 groups with aspect ratios H/B ranging from 4 to 15. More specifically, 3 different blocks for each of the 12 H/B aspect ratios are investigated, yielding a total of 36 specimens. Due to material irregularities and geometrical imperfections, the blocks' actual geometrical dimensions might slightly differ from the nominal ones. Such incongruity, especially if occurring at the edges [38], could cause an asymmetric response behaviour between the two rocking signs of rotation. In order to take into account such effects, the experimental parameters describing the actual properties of the system (i.e. p and α) are herein extracted distinctly for each sign of rotation by leveraging the relationship between the amplitude and the period of motion (Eq. (2)) [30].

Figure 1c schematically shows the main components of the free-rocking experimental setup. More specifically, it consists of a bottom block fixed on a rigid base, and a top block standing free on the former constitutes the structure under investigation. The free-rocking motion is activated in two steps. Firstly, an initial positive rotation θ_{xx} larger than the critical slenderness angle α^+ is imposed on the block (Figure 1a). Secondly, a threaded rod, which is locally in contact with the top of the block, is screwed, triggering the initiation of free-rocking motion with an initial condition of almost zero angular velocity [25]. The free-rocking motion is recorded by a Digital Image Correlation (DIC) system. The DIC is a contactless optical technique that allows the recording of the displacement field over time, with the advantage of avoiding any physical interference that might affect the dynamics of the system. Four cameras record the motion of the two faces of the block in the yz plane (Figure 1c), with a sampling frequency of 145 Hz. Figure 1b illustrates the preliminary preparation of the block surfaces,

which is characterised by a speckle pattern made of randomly distributed dots in greyscale and of uniform size (calibrated with respect to the camera's field of view). From each surface i and j shown in Figure 1c, the displacement time histories of two vertically aligned points (P1 and P2) are extracted (Figure 1b). Assuming rigid body motion, the displacement over time of the four points allows the estimation of the three rotations over the x-x, y-y and z-z axes as follows.

The rocking rotation over the x-x axis θ_{xx} is estimated as:

$$\theta_{xx,i} = \sin^{-1} \left(\frac{y_{i,top} - y_{i,bottom}}{dH} \right) \quad (7)$$

where $y_{i,top}$ and $y_{i,bottom}$ are the displacements in the y direction of the top and bottom points of the surface i , and dH is their relative vertical distance. Similarly, θ_{xx} is calculated for the surface j , while the final θ_{xx} is the average of the rotations of the two surfaces.

The rotation over the y-y axis θ_{yy} is estimated as:

$$\theta_{yy,top} = \sin^{-1} \left(\frac{z_{i,top} - z_{j,top}}{L} \right) \quad (8)$$

where $z_{i,top}$ and $z_{j,top}$ are the displacements in z direction of the top points of surface i and j , respectively, whereas L is the length of the block. Similarly, θ_{yy} is estimated for the bottom points, while the final θ_{yy} is the average of the top and bottom points.

The rotation over the z-z axis θ_{zz} is estimated as:

$$\theta_{zz,top} = \sin^{-1} \left(\frac{x_{i,top} - x_{j,top}}{L} \right) \quad (9)$$

where $x_{i,top}$ and $x_{j,top}$ are the displacements in x direction of the top points of surface i and j , respectively. Similarly, θ_{zz} is evaluated using the bottom points, and the final θ_{zz} is estimated as the average of the top and bottom points.

Finally, the energy loss during the free-rocking motion is quantified using the CoR. Experimentally, the CoR is preferably estimated using the energy balance of Eqs. (3-5), rather than directly using the ratio of angular velocities after and before each impact. More specifically, assuming that energy is preserved during the pivoting (i.e. smooth rocking) phase, the kinetic energy at impact (Eq. (4)) can be equated with the potential energy at the peak response of the corresponding half cycle (Eq. (3)), as they are alternatively nullified. This deliberate choice stems from two main reasons [25,30,35]: i) the DIC acquisition system directly measures displacements, which are consequently experimentally more reliable than velocities (which are computed as the gradient of displacements), and ii) instances of maximum rotations are captured with higher fidelity than instances of impacts, considering a constant sampling acquisition frequency of 145 Hz, and the high velocities of the system around impact. For the general case of asymmetric response, the results of each sign of rotation are preferably analysed. Therefore, the CoR is estimated as:

$$e = \sqrt{\sqrt{\frac{E_{\text{POTENTIAL, peak},i}}{E_{\text{POTENTIAL, peak},i+2}}}} \quad (10)$$

where $E_{\text{POTENTIAL, peak},i}$ and $E_{\text{POTENTIAL, peak},i+2}$ are the potential energies at time instances of peak responses i and $i+2$. In Eq. (10), the first square root derives from the squared angular velocity (Eq. (4)), while the second one is introduced since two impacts separate the peak responses i and $i+2$.

4 RESULTS

Figure 2 presents the response time history of a representative free-rocking test performed with a block of aspect ratio $H/B=5$. In detail, Figure 2a shows the rotational response over the x-x axis θ_{xx} , which constitutes the preeminent rocking response. θ_{xx} starts from an initial rotation equal to the critical slenderness angle, while the end of the motion is assumed to occur when an uncertainty threshold is reached, displayed in Figure 2 with a dashed line. Such threshold aims to delineate the boundary of reliable acquired response and it is defined

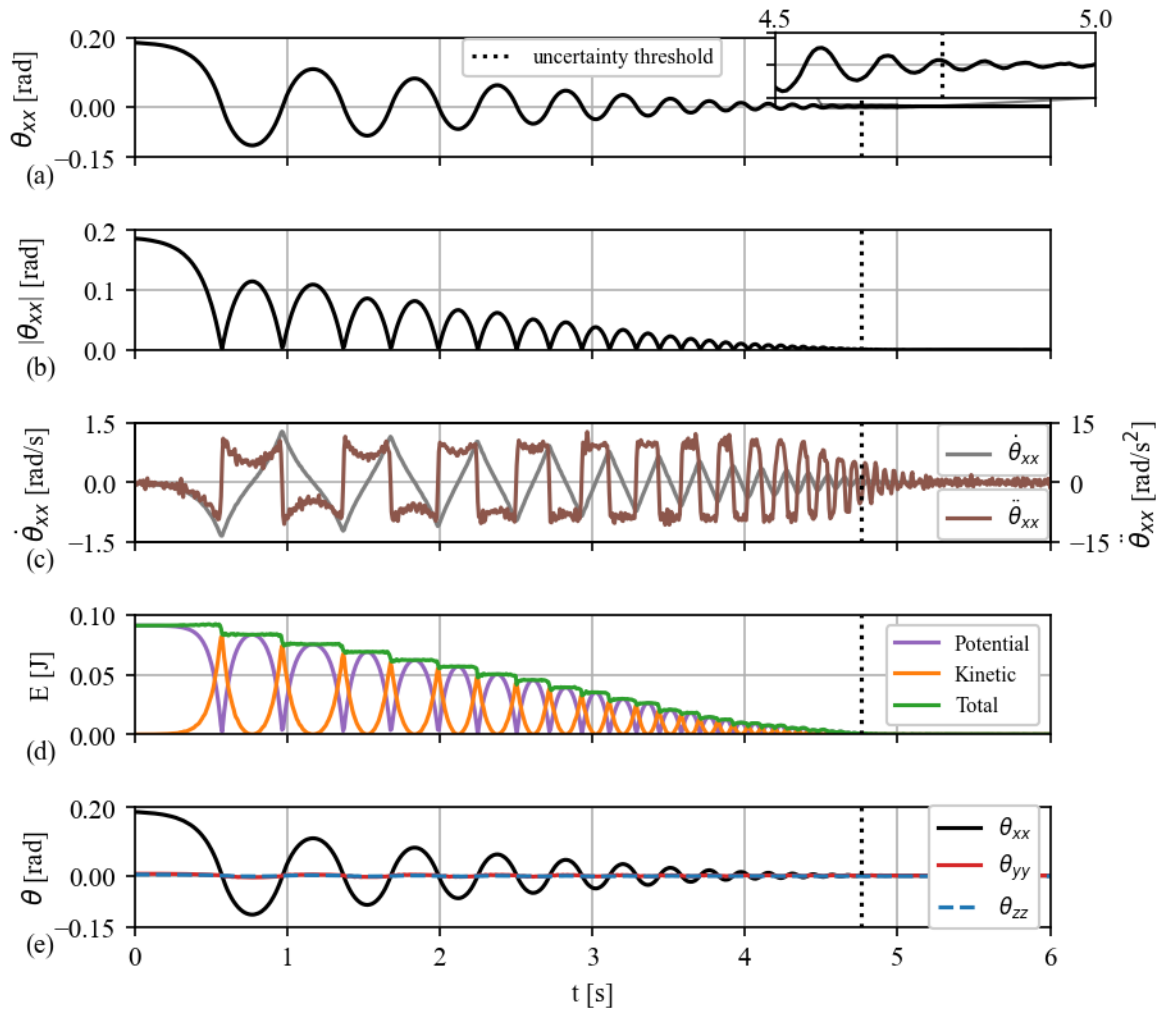


Figure 2: Response time histories in terms of (a) rotation over the x-x axis, (b) absolute rotation over the x-x axis, (c) angular velocity and angular acceleration over the x-x axis, (d) potential, kinetic and total energies, and (e) rotation over the x-x, y-y, and z-z axes.

assuming the ratio between the uncertainty value, recorded by the DIC system, and the amplitude of the rotation θ_{xx} to be less than 10%. Figure 2b plots the absolute value of the rocking angle θ_{xx} , where a modest asymmetric response can be observed. This phenomenon may be attributed to one or a combination of several factors, such as the presence of irregular contact interfaces, geometrical defects, a non-centred centre of mass, inclination of the bottom block etc. Figure 2c reports the angular velocity $\dot{\theta}_{xx}$ and angular acceleration $\ddot{\theta}_{xx}$ response time histories, obtained from the first and second numerical derivatives of the rotation θ_{xx} , respectively. The angular velocity $\dot{\theta}_{xx}$ shows a rather linear trend, which gradually decreases its amplitude over time. Its value becomes zero when the rotation θ_{xx} becomes maximum, while its maximum value occurs during impact. The angular acceleration $\ddot{\theta}_{xx}$ response is approximately constant during the pivoting (smooth rocking) phase, except for an internal oscillation caused by the cumulative noise introduced by the double derivatives, while it changes its sign suddenly at each impact. Figure 2d shows the experimentally measured energy balance of rocking motion (Eqs (3-5)). For each cycle, the $|\theta_{xx}|$ amplitude peaks correspond to a maximum potential energy and zero kinetic energy, with the latter reaching its maximum during impact. Overall, the total energy reduces with a stepwise fashion, i.e. being constant during the pivoting and experiencing abrupt reductions during impacts, thus being perfectly in line with the theoretical rocking dynamics [24]. Importantly, as the total energy remains constant during the pivoting (smooth rocking) phase, it appears reasonable to compute the CoR using the potential energy as per Eq. (10). Finally, Figure 2e depicts the rotations of the block in all three axes, x-x, y-y and z-z, where it is clearly shown that the θ_{xx} is the main component of motion, while θ_{yy} and θ_{zz} present negligible values.

Figure 3 illustrates with dots the experimental maximum amplitude $|\theta_{xx}|$ of each half cycle versus the corresponding period for the representative test of Figure 2, separately for positive and negative oscillations. Note that the first half cycle is omitted since it might include small interferences triggered by the screwing device. The experimental parameters p and α are estimated as the best fit resulting from the minimisation of the error between the amplitude-period law (Eq. (2)) and the experimental data. The outcomes of the fitted p and α parameters are shown in Table 1 and plotted in Figure 3, together with the values for nominal geometry

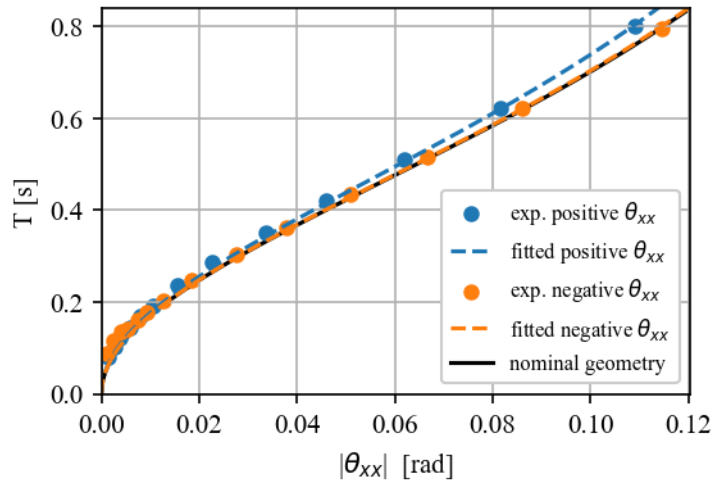


Figure 3: Period-amplitude dependency: experimental versus nominal geometry.

Table 1: Nominal and experimental parameters α and p .

	α [rad]	diff. [%]	p [Hz]	diff [%]
Nominal	0.197	-	7.597	-
Experimental positive $\dot{\theta}_{xx}$	0.187	5.5	7.595	0.0
Experimental negative $\dot{\theta}_{xx}$	0.197	0.3	7.597	0.0

(i.e. ideal) geometry. Table 1 indicates that the experimentally computed frequency parameter p perfectly resembles its nominal value for both signs of rotation, with a maximum difference of 0.02 % for the positive sign, while the slenderness angle α shows a minor difference of 5.5 % and 0.3 % for the positive and negative signs, respectively. Overall, the experimental period-amplitude data appears to follow closely the form of Eq. (2) and indicates a small asymmetry of the block between its two signs of rotation.

Figure 4a illustrates the experimentally estimated CoR values versus the maximum angular velocity $\dot{\theta}_{xx}$ of each corresponding cycle, for the representative test previously presented. Note that Figure 5a shows the evolution of the test starting from the right side of the graph and evolves towards the left side, following the reduction of the angular velocity. Moreover, Figure 4a plots the CoR given by Eq. (6), which is based on the assumption of conservation of angular momentum and is constant throughout the response time history. However, Figure 4a shows a non-constant trend of the experimental CoR that rather presents a gradual decrease over time with a scattered distribution at the end of the response. Nevertheless, the experimental CoR does not differ significantly from the theoretical CoR of Eq. (6). Finally, Figure 4b plots the experimental CoR values coming from all the 36 free-rocking tests performed herein. In addition, Figure 4b collects the experimentally measured CoR values found in the literature [20,26,30,31,34,36,41–46], together with the theoretical CoR computed using Eq. (6). Overall, Figure 4b shows that the 36 free-rocking tests follow the theoretical prediction of Eq. (6) up to an aspect ratio H/B of 12, while for higher aspect ratios the experimental outcomes indicate a smaller CoR. This discrepancy probably arises

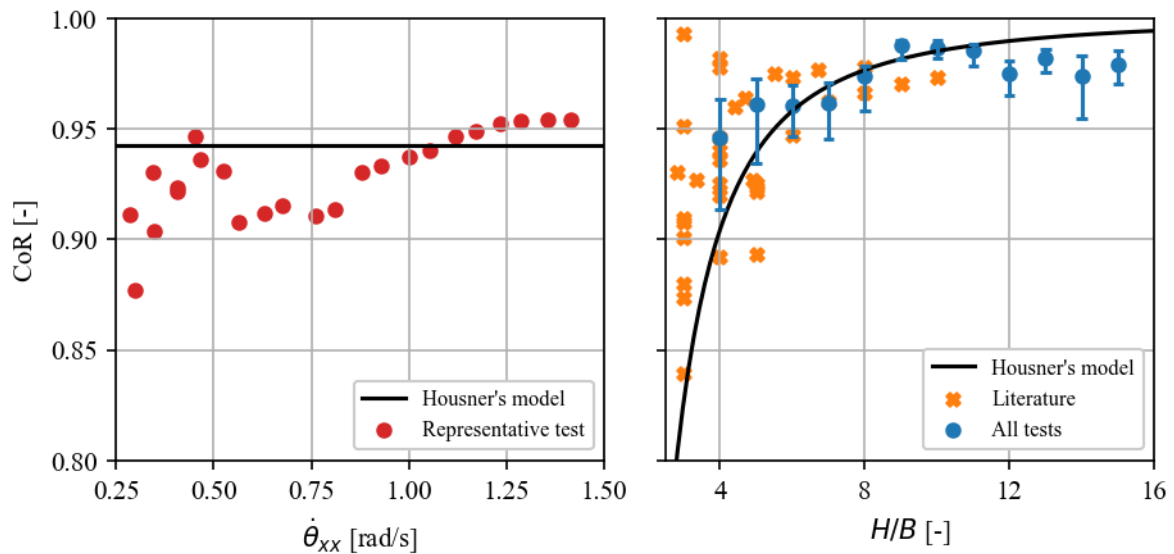


Figure 4: (a) Experimental versus Housner's theoretical CoR values for a representative free-rocking test, and (b) comparison of the CoR values estimated for all the 36 free-rocking tests with pertinent values from the literature [20,26,30,31,34,36,41–46] and Housner's model of Eq. (6) [13].

either due to the violation of the assumption of elastic impact behind Eq. (6) (i.e. no plastic deformation occurs at the surface asperities) or due to the presence of three-dimensional motion. Furthermore, the experimental results show a higher scatter for lower aspect ratios, with Eq. (6) providing a lower bound estimation. One potential explanation for this divergence has been provided by previous theoretical research [26–29] that highlighted that the impulsive forces during impact might not be concentrated solely at the corner pivot points. Nonetheless, the experimental CoR outcomes of this work lie within the scatter of the existing literature results for lower aspect ratios, while they provide novel experimental indications for higher aspect ratios, currently lacking from literature.

5 CONCLUSIONS

This paper presents an experimental characterisation of the free-rocking response of free-standing limestone blocks. The experimental campaign includes the investigation of 36 blocks, grouped into 12 aspect ratios (i.e. from 4 to 15) with three blocks for each group. Special attention is given to the energy dissipation mechanism at impacts, which is quantified via the coefficient of restitution (CoR), while the three-dimensional response, which is captured by a four-camera digital image correlation system, is also investigated.

The time history response of a representative test is firstly introduced and thoroughly discussed. The results show an oscillatory free-rocking behaviour, featured by modest asymmetry between the positive and negative rotations. Such an aspect is attributed to several sources of imperfection, which, however, are found to be of negligible interest given the very close resemblance between the nominal and experimental geometrical parameters, i.e. p and α . Overall, the planar rocking rotation θ_{xx} dominates the response compared to the other rotations (θ_{yy} , θ_{zz}), reinforcing the common assumption of planar rocking response.

Furthermore, particular emphasis is given to the experimental estimation of the energy losses during free-rocking motion through quantification of the CoR. The CoR values of a representative test appear to gradually decrease over time characterised by scattered values for small angular velocities – in contrast with Housner’s assumption of constant CoR throughout the response time history. Finally, a comprehensive comparison is made among the CoR values extracted from all the 36 free-rocking tests conducted herein, the experimental results gathered from the literature, and the theoretical CoR of Housner’s model. In general, the experimentally estimated CoR values follow the trend of the theoretical Housner’s model prediction. Specifically, the experimental results verify the high scatter of the CoR values observed in the literature for lower aspect ratios, while the CoR is underestimated for higher aspect ratios. Nevertheless, the results shown herein are part of a wider experimental investigation currently in progress aiming to provide a deeper insight into the estimation of the energy dissipation throughout the response time history and the complex nonlinear rocking phenomena.

REFERENCES

- [1] S. Lagomarsino, Seismic assessment of rocking masonry structures, *Bull. Earthq. Eng.* 13 (2015) 97–128. <https://doi.org/10.1007/s10518-014-9609-x>.
- [2] M. Aghagholizadeh, N. Makris, Seismic Response of a Yielding Structure Coupled with a Rocking Wall, *J. Struct. Eng.* 144 (2018) 1–13. [https://doi.org/10.1061/\(asce\)st.1943-541x.0001894](https://doi.org/10.1061/(asce)st.1943-541x.0001894).

- [3] A.I. Giouvanidis, Y. Dong, Seismic loss and resilience assessment of single - column rocking bridges, *Bull. Earthq. Eng.* (2020). <https://doi.org/10.1007/s10518-020-00865-5>.
- [4] E.G. Dimitrakopoulos, A.I. Giouvanidis, Seismic response analysis of the planar rocking frame, *J. Eng. Mech.* 141 (2015) 04015003. [https://doi.org/10.1061/\(ASCE\)EM.1943-7889.0000939](https://doi.org/10.1061/(ASCE)EM.1943-7889.0000939).
- [5] A. Agalianos, A. Psychari, M.F. Vassiliou, B. Stojadinovic, I. Anastasopoulos, Comparative assessment of two rocking isolation techniques for a motorway overpass bridge, *Front. Built Environ.* 3 (2017) 1–19. <https://doi.org/10.3389/fbuil.2017.00047>.
- [6] A.I. Giouvanidis, E.G. Dimitrakopoulos, Seismic Performance of Rocking Frames with Flag-Shaped Hysteretic Behavior, *J. Eng. Mech.* 143 (2017). [https://doi.org/10.1061/\(ASCE\)EM.1943-7889.0001206](https://doi.org/10.1061/(ASCE)EM.1943-7889.0001206).
- [7] I.M. Thomaidis, A.J. Kappos, A. Camara, Dynamics and seismic performance of rocking bridges accounting for the abutment-backfill contribution, *Earthq. Eng. Struct. Dyn.* (2020) 1–19. <https://doi.org/10.1002/eqe.3283>.
- [8] N. Reggiani Manzo, M.F. Vassiliou, Cyclic tests of a precast restrained rocking system for sustainable and resilient seismic design of bridges, *Eng. Struct.* 252 (2022). <https://doi.org/10.1016/j.engstruct.2021.113620>.
- [9] I.N. Psycharis, M. Fragiadakis, I. Stefanou, Seismic reliability assessment of classical columns subjected to near-fault ground motions, *Earthq. Eng. Struct. Dyn.* 42 (2013) 2061–2079. <https://doi.org/10.1002/eqe.2312>.
- [10] S. Diamantopoulos, M. Fragiadakis, Modeling, fragility and risk assessment of ancient freestanding columns and colonnades, *Eng. Struct.* 275 (2023). <https://doi.org/10.1016/j.engstruct.2022.115273>.
- [11] L. Sorrentino, L. Liberatore, D. Liberatore, R. Masiani, The behaviour of vernacular buildings in the 2012 Emilia earthquakes, *Bull. Earthq. Eng.* 12 (2014) 2367–2382. <https://doi.org/10.1007/s10518-013-9455-2>.
- [12] A. Mehrotra, M.J. DeJong, The influence of interface geometry, stiffness, and crushing on the dynamic response of masonry collapse mechanisms, *Earthq. Eng. Struct. Dyn.* 47 (2018) 2661–2681. <https://doi.org/10.1002/eqe.3103>.
- [13] A. Di Egidio, A. Contento, Base isolation of slide-rocking non-symmetric rigid blocks under impulsive and seismic excitations, *Eng. Struct.* 31 (2009) 2723–2734. <https://doi.org/10.1016/j.engstruct.2009.06.021>.
- [14] A. Mauro, G. de Felice, M.J. DeJong, The relative dynamic resilience of masonry collapse mechanisms, *Eng. Struct.* 85 (2015) 182–194. <https://doi.org/10.1016/j.engstruct.2014.11.021>.
- [15] O. Al Shawa, G. De Felice, A. Mauro, L. Sorrentino, Out-of-plane seismic behaviour of rocking masonry walls, *Earthq. Eng. Struct. Dyn.* 41 (2012) 949–968. <https://doi.org/10.1002/eqe.1168>.
- [16] G. Vlachakis, E. Vlachaki, P.B. Lourenço, Learning from failure: Damage and Failure of Masonry Structures, after the 2017 Lesvos Earthquake (Greece), *Eng. Fail. Anal.* 117 (2020) 104803. <https://doi.org/10.1016/j.engfailanal.2020.104803>.
- [17] L. Sorrentino, S. Cattari, F. da Porto, G. Magenes, A. Penna, Seismic behaviour of

- ordinary masonry buildings during the 2016 central Italy earthquakes, *Bull. Earthq. Eng.* 17 (2019) 5583–5607. <https://doi.org/10.1007/s10518-018-0370-4>.
- [18] N. Makris, A half-century of rocking isolation, *Earthq. Struct.* 7 (2014) 1187–1221. <https://doi.org/10.12989/eas.2014.7.6.1187>.
- [19] A.I. Giouvanidis, E.G. Dimitrakopoulos, P.B. Lourenço, Chattering: An overlooked peculiarity of rocking motion, *Nonlinear Dyn.* 109 (2022) 459–477. <https://doi.org/10.1007/s11071-022-07578-1>.
- [20] J.A. Bachmann, M. Strand, M.F. Vassiliou, M. Broccardo, B. Stojadinović, Is rocking motion predictable?, *Earthq. Eng. Struct. Dyn.* 47 (2018) 535–552. <https://doi.org/10.1002/eqe.2978>.
- [21] M.N. Chatzis, A.W. Smyth, Robust Modeling of the Rocking Problem, *J. Eng. Mech.* 138 (2012) 247–262. [https://doi.org/10.1061/\(ASCE\)EM.1943-7889.0000329](https://doi.org/10.1061/(ASCE)EM.1943-7889.0000329).
- [22] G. Vlachakis, A.I. Giouvanidis, A. Mehrotra, P.B. Lourenço, Numerical block-based simulation of rocking structures using a novel universal viscous damping model, *J. Eng. Mech.* 147 (2021) 04021089. [https://doi.org/10.1061/\(ASCE\)EM.1943-7889.0001985](https://doi.org/10.1061/(ASCE)EM.1943-7889.0001985).
- [23] A.I. Giouvanidis, E.G. Dimitrakopoulos, Nonsmooth dynamic analysis of sticking impacts in rocking structures, *Bull. Earthq. Eng.* 15 (2017) 2273–2304. <https://doi.org/10.1007/s10518-016-0068-4>.
- [24] G. Housner, The behavior of inverted pendulum structures during earthquakes, *Bull. Seismol. Soc. Am.* 53 (1963) 403–417. <https://doi.org/10.1017/CBO9781107415324.004>.
- [25] L. Sorrentino, O. AlShawa, L.D. Decanini, The relevance of energy damping in unreinforced masonry rocking mechanisms. Experimental and analytic investigations, *Bull. Earthq. Eng.* 9 (2011) 1617–1642. <https://doi.org/10.1007/s10518-011-9291-1>.
- [26] D. Kalliontzis, S. Sritharan, A. Schultz, Improved Coefficient of Restitution Estimation for Free Rocking Members, *J. Struct. Eng.* (2016) 1–7. [https://doi.org/10.1061/\(ASCE\)ST.1943-541X.0001598](https://doi.org/10.1061/(ASCE)ST.1943-541X.0001598).
- [27] T. Ther, L.P. Kollar, Refinement of Housner’s model on rocking blocks, *Bull. Earthq. Eng.* 15 (2017) 2305–2319. <https://doi.org/10.1007/s10518-016-0048-8>.
- [28] M.N. Chatzis, M.G. Espinosa, A.W. Smyth, Examining the Energy Loss in the Inverted Pendulum Model for Rocking Bodies, *J. Eng. Mech.* 143 (2017). [https://doi.org/10.1061/\(ASCE\)EM.1943-7889.0001205](https://doi.org/10.1061/(ASCE)EM.1943-7889.0001205).
- [29] H. Zhu, M.N. Chatzis, S. Acikgoz, A new impact model for the flexible rocking oscillator, *Earthq. Eng. Struct. Dyn.* 51 (2022) 1819–1839. <https://doi.org/10.1002/eqe.3639>.
- [30] F. Peña, P.B. Lourenço, A. Campos-Costa, Experimental dynamic behavior of free-standing multi-block structures under seismic loadings, *J. Earthq. Eng.* 12 (2008) 953–979. <https://doi.org/10.1080/13632460801890513>.
- [31] P.R. Lipscombe, S. Pellegrino, Free Rocking of Prismatic Blocks, *J. Eng. Mech.* 119 (1993) 1387–1410. [https://doi.org/10.1061/\(ASCE\)0733-9399\(1993\)119:7\(1387\)](https://doi.org/10.1061/(ASCE)0733-9399(1993)119:7(1387)).
- [32] D. Konstantinidis, N. Makris, Experimental and analytical studies on the response of

- freestanding laboratory equipment to earthquake shaking, *Earthq. Eng. Struct. Dyn.* 38 (2009) 827–848. <https://doi.org/10.1002/eqe.871>.
- [33] P.L. Várkonyi, M. Kocsis, T. Ther, Rigid impacts of three-dimensional rocking structures, *Nonlinear Dyn.* 107 (2022) 1839–1858. <https://doi.org/10.1007/s11071-021-06934-x>.
- [34] M. ElGawady, Q. Ma, J. Butterworth, J. Ingham, Effects of interface material on the performance of free rocking blocks, *Earthq. Eng. Struct. Dyn.* 40 (2011) 375–392. <https://doi.org/10.1002/eqe.1025>.
- [35] A.A. Costa, A. Arêde, A. Penna, A. Costa, Free rocking response of a regular stone masonry wall with equivalent block approach: experimental and analytical evaluation, *Earthq. Eng. Struct. Dyn.* 42 (2013) 2297–2319. <https://doi.org/10.1002/eqe.2327>.
- [36] P.D. Spanos, A. Di Matteo, A. Pirrotta, M. Di Paola, Rocking of rigid block on nonlinear flexible foundation, *Int. J. Non. Linear. Mech.* 94 (2017) 362–374. <https://doi.org/10.1016/j.ijnonlinmec.2017.06.005>.
- [37] D. Kalliontzis, S. Sritharan, Characterizing dynamic decay of motion of free-standing rocking members, *Earthq. Spectra.* 34 (2018) 843–866. <https://doi.org/10.1193/011217EQS013M>.
- [38] C. Mathey, C. Feau, I. Politopoulos, D. Clair, L. Baillet, M. Fogli, Behavior of rigid blocks with geometrical defects under seismic motion: an experimental and numerical study, *Earthq. Eng. Struct. Dyn.* 45 (2016) 2455–2474. <https://doi.org/10.1002/eqe.2773>.
- [39] P. Flores, Contact mechanics for dynamical systems: a comprehensive review, *Multibody Syst. Dyn.* 54 (2021) 127–177. <https://doi.org/10.1007/s11044-021-09803-y>.
- [40] G. Vlachakis, C. Colombo, A.I. Giouvanidis, N. Savalle, P.B. Lourenco, Experimental characterisation of dry-joint masonry structures: Interface stiffness and interface damping, *Constr. Build. Mater.* (2023). <https://doi.org/10.1016/j.conbuildmat.2023.130880>.
- [41] M. Aslam, W.G. Godden, D.T. Scalise, *Earthquake Rocking Response of Rigid Bodies*, 1978.
- [42] M.J.N. Priestley, R.J. Evison, A.J. Carr, Seismic Response of Structures free to rock on their foundations, *Bull. New Zeal. Soc. Earthq. Eng.* 11 (1978) 141–150.
- [43] C.M. Wong, W.K. Tso, Steady state rocking response of rigid blocks part 2: Experiment, *Earthq. Eng. Struct. Dyn.* 18 (1989) 107–120. <https://doi.org/10.1002/eqe.4290180110>.
- [44] N. Ceh, G. Jelenic, B. Nenad, Analysis of restitution in rocking of single rigid blocks, *Acta Mech.* 229 (2018) 4623–4642. <https://doi.org/10.1007/s00707-018-2246-8>.
- [45] K. Muto, H. Umemura, Y. Sonobe, Study of the overturning vibration of slender structures, in: *Proc. Second World Conf. Earthq. Eng., Japan*, 1960.
- [46] N. Ogawa, A study on rocking and overturning of rectangular column, *Rep. Natl. Res. Cent. Disaster Prev.* 18 (1977).